Cancer Research

Mitochondrial Genomic Backgrounds Affect Nuclear DNA Methylation and Gene Expression

Carolyn J. Vivian[1,2], Amanda E. Brinker[1,2,3], Stefan Graw[4], Devin C. Koestler[4,5], Christophe Legendre[6], Gerald C. Gooden[6], Bodour Salhia[6], and Danny R. Welch[1,2,3,5]

Abstract

Mitochondrial DNA (mtDNA) mutations and polymorphisms contribute to many complex diseases, including cancer. Using a unique mouse model that contains nDNA from one mouse strain and homoplasmic mitochondrial haplotypes from different mouse strain(s)—designated Mitochondrial Nuclear Exchange (MNX)—we showed that mtDNA could alter mammary tumor metastasis. Because retrograde and anterograde communication exists between the nuclear and mitochondrial genomes, we hypothesized that there are differential mtDNA-driven changes in nuclear (n)DNA expression and DNA methylation. Genome-wide nDNA methylation and gene expression were measured in harvested brain tissue from paired wild-type and MNX mice. Selective differential DNA methylation and gene expression were observed between strains having identical nDNA, but different mtDNA. These observations provide insights into how mtDNA could be altering epigenetic regulation and thereby contribute to the pathogenesis of metastasis. *Cancer Res; 77(22); 6202–14. ©2017 AACR.*

Introduction

Mitochondria are cytoplasmic organelles that contain maternally inherited DNA and encode proteins central to cellular metabolism. The mitochondrial genome is ∼16,600 base pairs in humans and ∼16,300 base pairs in mice, and encodes 37 genes—13 proteins, 22 tRNA, and 2 rRNA. Mitochondrial DNA (mtDNA)-encoded proteins are necessary for oxidative phosphorylation. However, the vast majority of mitochondrial proteins are encoded within the nuclear genome. Despite its extraordinarily high sequence variability, which has been used to map human evolution (1–3), mtDNA has been traditionally thought to be relatively innocuous (4). Recent evidence strongly demonstrates that naturally occurring mtDNA polymorphisms are not neutral, and that mtDNA–nDNA interactions profoundly affect mammalian biology (5, 6) and contribute to some pathologies (7, 8).

mtDNA mutations and polymorphisms contribute to many complex diseases, including atherosclerosis (9), Alzheimer's disease (10, 11), diabetes (12), obesity (13), aging (5), and cancer (8, 14, 15). Although the mechanisms responsible remain mostly unknown, we hypothesized that there are differential mtDNA-driven changes in nuclear (n)DNA expression and DNA methylation, as retrograde and anterograde communication exists between the nuclear and mitochondrial genomes. After generating a unique mouse model that contains nDNA from one mouse strain and homoplasmic mitochondrial haplotypes from different mouse strain(s)—designated Mitochondrial Nuclear Exchange (MNX; refs. 7, 8, 16)—genome-wide nDNA methylation and gene expression were measured in harvested brain tissue.

Intuitively, retrograde communication from the mitochondria to the nucleus is crucial in sensing homeostasis and translating extracellular signals into altered gene expression (6). Mitochondria-directed changes in nuclear gene function (17) are presumably related to a mitochondrion's role in generating and regulating high energy molecules, such as ATP, acetyl-CoA, and α-ketoglutarate. Changes in nuclear gene expression reciprocally signal the mitochondrial genome (18, 19), regulating mitochondrial mass, bioenergetic state, and redox potential (20). Ultimately, cross-talk between genomes is vital for the proper maintenance, integrity, and function of both genomes and presumably contributes to the symbiotic relationship between them. Most knowledge of retrograde signaling comes from studies performed in *S. cerevisiae*, where it has been shown that the key regulatory pathways are dependent upon retrograde signaling (21, 22). Studies of this type have led to hypotheses that disruptions or mutations in one genome can result in epigenetic changes in the other genome (17).

The epigenome (the collective sum of all epigenetic information) contains hypervariable regions and is temporally and spatially regulated, such that there are as many epigenomes as there

[1]Department of Cancer Biology, University of Kansas Medical Center, Kansas City, Kansas. [2]Heartland Center for Mitochondrial Medicine, Phoenix, Arizona. [3]Department of Molecular and Integrative Physiology, University of Kansas Medical Center, Kansas City, Kansas. [4]Department of Biostatistics, University of Kansas Medical Center, Kansas City, Kansas. [5]The University of Kansas Cancer Center, University of Kansas Medical Center, Kansas City, Kansas. [6]Translational Genomics Research Institute, Phoenix, Arizona.

Note: Supplementary data for this article are available at Cancer Research Online (http://cancerres.aacrjournals.org/).

Current Address for B. Salhia: Norris Comprehensive Cancer Center, Keck School of Medicine, Department of Translational Genomics, The University of Southern California, Los Angeles, CA.

Corresponding Author: Danny R. Welch, The University of Kansas Medical Center, 3901 Rainbow Boulevard, Mailstop 1071, Kansas City, KS 66160-2937. Phone: 913-945-7739; E-mail: dwelch@kumc.edu

doi: 10.1158/0008-5472.CAN-17-1473

are cell types (23) and cell states (24, 25). DNA methylation is the most extensively characterized epigenetic mechanism (26, 27). This covalent modification is usually found at cytosine residues within CpG dinucleotides and is catalyzed by DNA methyltransferase (DNMT). In most human tissues, the vast majority of the genome is highly methylated (>70%), including at repetitive sequences (26, 28), gene bodies (26, 29, 30), and other regulatory regions. Most often, methylation occurs within CpG dinucleotides. Clusters of CpG loci form islands (CPGI), which when located in promoters, are normally unmethylated and allow open transcription of important and often cancer-inhibiting genes. Methylated DNA promotes the recruitment of methyl-CpG–binding domain proteins, which, in turn, generally suppresses transcription of genes involved in processes such as embryonic development, genomic imprinting, X-chromosome inactivation, and chromosome stability (31–35). Similarly, methylation of mtDNA has been reported (36), but acceptance of those findings is not universal (37). Therefore, in this report, we refer only to the nuclear epigenome in terms of describing its characteristics.

There are relatively few diseases caused directly by mitochondrial mutations or polymorphisms (38, 39). In most cancers, mtDNA polymorphisms are not considered to be "drivers" of tumorigenicity (38, 40, 41). Rather, they are among many genes influencing disease susceptibility, progression, and severity (40–42). Similarly, as observed in other complex traits, even reproducible findings in one individual may not apply to another because of interindividual heterogeneity. For example, had researchers exclusively used the DBA/2J instead of the C57BL/6J mouse strain, they would have mistakenly concluded that morphine is neither addictive nor a painkiller (41). In addition to nuclear genomic differences, mitochondrial dysfunction has been associated with complex diseases and dramatically affects disease susceptibility and severity, suggesting a relationship between the mitochondrial and nuclear genomes, which perhaps involves DNA methylation (43).

In the mouse, the nuclear genome consists of approximately 38,000 CPGI affecting 18,000 genes, and 2.5 million SNP (44). To study the role of mtDNA on nDNA epigenetics, we utilized MNX mice in which the nuclear genome from one mouse strain is combined with mtDNA from different strains of mice (7, 8). Briefly, MNX mice were generated by enucleating oocytes from strain A and transferring nuclei from strain B to replace the removed nucleus (Fig. 1). Nucleated oocytes were then transplanted back into a pseudopregnant female of the appropriate strain. Strain identities were verified using PCR and/or restriction fragment length polymorphisms within nDNA and mtDNA. Mice were also confirmed to be homoplasmic for mtDNA before using them for experimental studies. These new mouse strains have been successfully bred and phenotypes have remained stable over many generations. We previously showed, using the MNX mice, that susceptibility to atherosclerosis (7) as well as breast tumor formation and metastasis (8) are profoundly affected by mtDNA SNP when bred to genetically engineered male mice carrying oncogenes. By changing the mitochondrial background, we observed a change in tumor onset and size and number of metastases, indicating that the mitochondrial genome can potentially influence the microenvironment of the tumor cells. As these, like all other complex diseases, require coordinated expression of many nuclear genes and because cross-talk and epigenetic effects exist between the two genomes, we chose to investigate the effects of the mitochondrial genome on nuclear genome methylation using an unbiased genome-wide approach in order to begin exploring possible mechanisms for the observed biology.

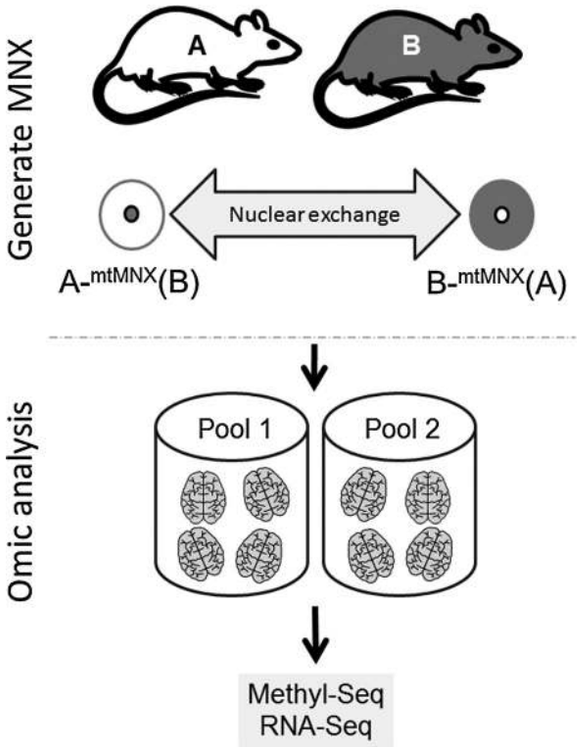

Figure 1.
Generation of MNX mice and experimental design. Schematic diagram depicting generation of MNX mice by enucleation of oocytes and transfer of the nucleus from another strain into the oocytes of the recipient strain. Brains were collected from male mice (8 weeks) originating from four separate cages from both wild-type and MNX strains. A piece of brain tissue (5–8 mg), mostly cerebellum, was cut from four samples and pooled together into a tube for DNA and RNA extraction for Methyl-Seq and RNA-Seq analyses.

Materials and Methods

Mice

We utilized four different MNX strains and their wild-type counterparts that share the same nuclear background, resulting in eight different strains. We refer to each strain with nuclear component listed first and the mitochondrial component listed second. MNX mice were created as previously reported (7, 8). The approved nomenclature is written with the nuclear contribution followed by the mitochondrial contributor in parentheses. To distinguish MNX mice from conplastic mice, "MNX" is included. The following four MNX strains were generated: FVB/NJ-$^{mtMNX(C57BL/6)}$, FVB/NJ -$^{mtMNX(BALB/cJ)}$, C3H/HeN-$^{mtMNX(C57BL/6J)}$, C57BL/6J-$^{mtMNX(C3H/HeN)}$, along with their wild-type counterparts: FVB/NJ, C3H/HeN, C57BL/6J, BALB/cJ. For simplicity in this article, these mouse strains will be abbreviated as listed in the right-hand column of Table 1. Wild-type FVB/NJ (FF), BALB/cJ (BB), and C57BL/6J (CC) mice were purchased from Jackson Laboratories and C3H/HeN (HH) wild-type mice were purchased from Envigo (formerly Harlan Laboratories). All wild-type mice were purchased from the

Table 1. Mitochondria-nuclear exchange mouse strains

Mouse strain (official nomenclature)	Nuclear DNA	Mitochondrial DNA	Abbreviation
FVB/NJ-$^{mtMNX(FVB/NJ)}$	FVB/NJ	FVB/NJ	FF
FVB/NJ -$^{mtMNX(C57BL/6J)}$	FVB/NJ	C57BL/6J	FC
FVB/NJ -$^{mtMNX(BALB/cJ)}$	FVB/NJ	BALB/cJ	FB
BALB/cJ-$^{mtMNX(BALB/cJ)}$	BALB/cJ	BALB/cJ	BB
C57BL/6J -$^{mtMNX(C57BL/6J)}$	C57BL/6J	C57BL/6J	CC
C57BL/6J-$^{mtMNX(C3H/HeN)}$	C57BL/6J	C3H/HeN	CH
C3H/HeN-$^{mtMNX(C57BL/6J)}$	C3H/HeN	C57BL/6J	HC
C3H/HeN-$^{mtMNX(C3H/HeN)}$	C3H/HeN	C3H/HeN	HH

NOTE: MNX mice were generated by enucleating oocytes from strain A and transferring nuclei from strain B to replace the removed nucleus. Nucleated oocytes were then transplanted back into a pseudopregnant female of the appropriate strain. A schematic diagram for mouse development is shown in Fig. 1. Previous studies showed that MNX mice created with wild-type mtDNA with the same nuclear background behaved identically to traditionally bred wild-type mice.

vendor and housed at least 2 weeks in the KUMC facility until time of harvest. The MNX mice underwent continuous breeding to maintain the lines. Multiple mating pairs were set up and the males from the litters were used to harvest the brains at 8 weeks of age. MNX mice were at the 8th filial generation. MNX colonies were maintained by crossing the MNX females with males of identical nuclear background. Mice were bred, weaned, and aged to 8 weeks. Each MNX and wild-type mouse were housed in a separate cage. All animal studies were approved by the Institutional Animal Care and Use Committee at the University of Kansas Medical Center.

Genotyping

Mitochondrial haplotypes of first generation MNX mice were confirmed by whole mitochondrial genome sequencing and compared with established wild-type strains. The mtDNA haplotypes from subsequent generations of MNX mice were confirmed by RFLP (restriction fragment length polymorphism) analysis of PCR products using SNP that are distinguishable between the strains. Mouse DNA were subjected to 35 to 40 cycles of PCR and gels were overexposed to maximize detection of heteroplasmy. FVB/NJ and C57BL/6J were distinguished by a C to T mutation at mtDNA position 9461, resulting in the loss of the BclI restriction site. FVB/NJ and BALB/cJ were distinguished by the G to A mutation at mtDNA position 9348 containing a PflFI restriction site. C57BL/6J and C3H/HeN were distinguished by the A to G mutation at mtDNA position 9348 containing a PflFI restriction site. All mice used for these studies were confirmed homoplasmic.

Tissue harvest

At 8 weeks of age, the male wild-type and male MNX mice were euthanized and the brains were harvested, flash frozen in liquid nitrogen and then stored at −80°C. DNA and RNA from MNX mice and wild-type mice were harvested from brain, using mostly cerebellum, from 8 independent males. Four different male mice housed in four different cages were separated and two replicate biological pools were created.

Genomic DNA extraction and Methyl-Seq

Libraries for sequencing were prepared for each pool of 4 brains using the SureSelect Methyl-Seq Target Enrichment System (Cat# G9651A, Agilent). Three micrograms of input DNA per pool were fragmented to an average size of 150 to 200 bp using the Covaris S2 system. Subsequent end repair, 3′ dA tailing, and methylated-adaptor ligation were performed according to the manufacturer's recommended protocol. DNA (750 ng) was used for hybridization/capture with SureSelect Mouse Methyl-Seq (Cat# 931052, Agilent) baits. This system enables a genome-wide, capture-based, mouse-specific, and bisulfite-based method to analyze nDNA methylation. This platform is analogous to the commercially available SureSelect Human Methyl-Seq Kit. This method allows for the characterization of DNA methylation status of over 3 million CpG in islands, shores, undermethylated regions, promoters, and differentially methylated regions (DMR) at single base-pair resolution using a 2×10^9 Mb sequencing design. For DNA library preparation, 3 μg of input DNA from fresh-frozen tissue underwent shearing, end repair, methylated adapter ligation, bisulfite treatment, PCR and sequencing according to the manufacturer's guidelines. Briefly, postcapture bisulfite conversion using the EZ DNA Methylation-Gold Kit (Cat# D5005, Zymo) was performed according to manufacturer's protocol, followed by an 8-cycle PCR amplification. A 6-cycle indexing PCR and cleanup were performed following Agilent's SureSelect Methyl-Seq standard protocol. Final library QC was conducted using BioAnalyzer DNA 1000 chips (Agilent) and the Qubit dsDNA High Sensitivity fluorometric assay (Invitrogen). An equimolar pool of 16 libraries was created at a concentration of 5 nmol/L. The pool was subsequently diluted and clustered on the Illumina cBot, using TruSeq Paired End Cluster Kit v.3 chemistry. Paired-end sequencing for the pool was carried out over 8 lanes on the Illumina HiSeq 2500 platform using TruSeq SBS v3 kits, for a total read length of 200 bp.

Methyl-Seq data processing and analysis

Bisulfite-modified DNA reads from WGBS and MiSeq were aligned to the bowtie2-indexed reference genome mm9 using Bismark tool version 0.12.7. Bismark relies on two external tools, bowtie (http://bowtie-bio.sourceforge.net/index.shtml) and Samtools (http://www.htslib.org). We respectively used bowtie2 version 2.0.0-beta6, and Samtools version 0.1.19. Bismark was used as suggested except for the bowtie2's parameter N (number of mismatches in a seed alignment during multispeed alignment) where the value of 1 was used for increased sensitivity. Next, PCR duplicates were removed for WGBS using default parameters. Methylation calling was also processed using a Bismark module called "Methylation Extractor," which was used according to the author's specifications. The output SAM files were merged manually for each of the biological replicate results. Base-pair level differential methylation analysis was implemented using the R package methylKit 0.9.2. Bismark's sam file output was used as input to methylKit (45) and data imported using the embedded function "read.bismark." The minimum read coverage and phred quality to call a methylation status for a CpG locus were both set to 20. The read.context option was set to "CpG." Other options to read.bismark function were set to default values. Eleven pair-wise comparisons were performed in methylKit using the Fisher exact test. Before calling differential methylation, each comparison was methylKit-reorganized, united, and then underwent differential methylation analysis using methylKit functions. Loci with differential methylation values (DMV) $\geq$ 20 (in percent scale) and q values <0.05 were considered differentially methylated loci (DML). A q value is a P value that has been adjusted for the false discovery rate (FDR). MethylKit DMLs were annotated according

to genomic landmarks as often used by Illumina genomic annotations for methylation analysis: Gene Body, TSS1500, Exon1, 5-prime UTR, 3-prime UTR, CpG Island (CPGI), and OpenSea. CPGI islands, Exon1, 5-prime UTR, and 3-prime UTR coordinates were extracted from the UCSC website for the mm9 genome. Transcriptional start site (TSS)1500 are loci situated 1,500 bases upstream to the TSS. Gene Body regions are defined from the Start Codon to the Stop codon, including introns. OpenSea are regions that do not fall in any of the above coordinates.

RNA extraction and RNA-Seq

Total RNA was isolated from the same male mouse brain tissues using RNeasy Lipid Tissue Mini Kit (Qiagen). Briefly, brain tissue was homogenized in Qiazol and centrifuged at >8,000 × g before adding chloroform and centrifuging (12,000 ×g), DNase treatment, washing in 75% ethanol and re-suspending the pellet in RNase free water. RNA quality was verified using an Agilent Bioanalyzer. RNA (1–2 μg) was used for RNASeq on an Illumina HiSeq 2500. Stranded total RNA libraries were prepared for each mouse strain. The libraries were then sequenced using Illumina HiSeq 2500 High Output with single read 100 bp and paired-end 100 bp. Genes with at least 1 count per million reads were considered "present" and the number of genes was identified in the data set. "Absent" genes were filtered from the analysis.

RNA-Seq data processing and biostatistics

The FastQC (0.11.2) software was used to assess the quality of the RNA sequencing results. Afterwards, RSEM (1.2.22) was used to align the reads to the reference genome mm9 and calculated the gene expression values. R (3.2.2) and EdgeR (3.12.0) were used to first normalize the expression values using the TMM-method (weighted trimmed mean of M values), followed by differential expression analyses. First, the negative binomial conditional common likelihood was maximized to estimate a common dispersion value across all genes (estimateCommonDisp). Next, tagwise dispersion values were estimated by an empirical Bayes method based on weighted conditional maximum likelihood (estimateTagwiseDisp). Finally, the differentially gene expression was calculated by computing the genewise exact tests for differences in the means between two groups of negative-binomially distributed counts.

To reduce the burden of multiple testing occurring in differential gene expression analysis, initially a filter was applied to reduce the number of genes. Genes were removed if they did not present a meaningful gene expression across all samples, only genes with cpm of >100 for at least two samples were considered in differential expression analysis. Also, the Benjamini and Hochberg procedure was used to control the FDR.

Normalized expression values were also used to perform a hierarchical cluster analysis and a principal component analysis (PCA). Hierarchical cluster analysis was determined using Euclidean distance. Two genes "Lars2" and "GU332589" were excluded from the analyses, because they exhibited an abnormal behavior. The following R-packages were utilized for calculations and visualizations: EdgeR, gplot, plotrix, grDevices, and colorfulVennPlot.

Methylation-specific PCR and bisulfite sequencing

Genomic DNA underwent bisulfite conversion using EZ DNA Methylation Kit (Zymo Research). Bisulfite converted DNA was then subjected to methylation-specific PCR using methylation specific primers. Methylation specific primers were designed using MethPrimer (46).

Quantitative PCR

Total RNA from the brain pools was used to synthesize cDNA. cDNA used to perform qPCR using Taqman assays for the following genes (Supplementary Fig. S1). Taqman assays were performed using ThermoFisher ViiA7 thermocyclers. Samples were normalized to β-actin.

Results

MNX and wild-type mice differ in brain tissue DNA methylation

We chose to study brain because it has abundant mitochondria (47) and because epigenetic modifications in brain tissues have already been implicated in modulating transcriptional changes that are important for synaptic connections and circuitry rewiring (28, 48). Our studies were performed using cerebella harvested at 8 weeks of age. Homoplasmic male mice were chosen to minimize the influences of hormonal changes associated with puberty and menstruation. Cerebella were harvested and collected in separate tubes, then pooled for DNA extraction. To mitigate issues of interindividual heterogeneity, brain tissues from eight different wild-type (FF, BB, CC, HH) or MNX (FC, FB, CH, HC) strains were harvested. Two replicate biological pools (Pools A and B) each contained four cerebella from age-matched mice from separate litters. Wild-type mice were purchased and were then housed in the KUMC animal facility until tissues were collected. (Note: Previous studies demonstrated that the nuclear transfer protocol used to generate MNX mice did not alter wild-type behaviors. This was expected as this procedure is used to generate most transgenic mouse models.) All MNX mice were maintained in the KUMC breeding colony. MNX and wild-type strains were housed in separate cages. MNX mice used for these studies were at the 8th filial generation following creation, eliminating the possibility of carry-over artifacts associated with the nuclear transfer. Genomic DNA extracted from both pools (Pools A and B—a total of 16 samples) was prepared for genome-wide DNA methylation next-generation sequencing using the Agilent SureSelect Mouse Methyl Seq library preparation method, which uses a capture-based approach to enrich target sequences specifically against the mouse methylome (Fig. 1). This is among the first reports (49) utilizing the mouse Methyl-Seq platform and the first to use it to analyze brain.

Quality control metrics for the DNA methylation data showed that there was good genomic coverage and that a high percentage of reads were above the threshold. Pearson correlations of CpG-specific DNA methylation ranged from 0.91 to 0.98 across strains, indicating a strong linear relationship in CpG-specific DNA methylation between the different strains (Fig. 2A). A PCA showed a clustering of samples based upon their first two principal components, primarily on the nDNA background with clear differences between MNX mice and the wild-type counterparts based upon specific combinations of nDNA and mtDNA (Fig. 2C). Duplication and alignment statistics for all 16 samples (two pools of 8 samples) using Bismark (45) showed that very few duplication alignments were found (Supplementary Fig. S2). Duplications that were identified were removed from further analyses. Most reads were sequence pairs and paired-end alignments with unique hits.

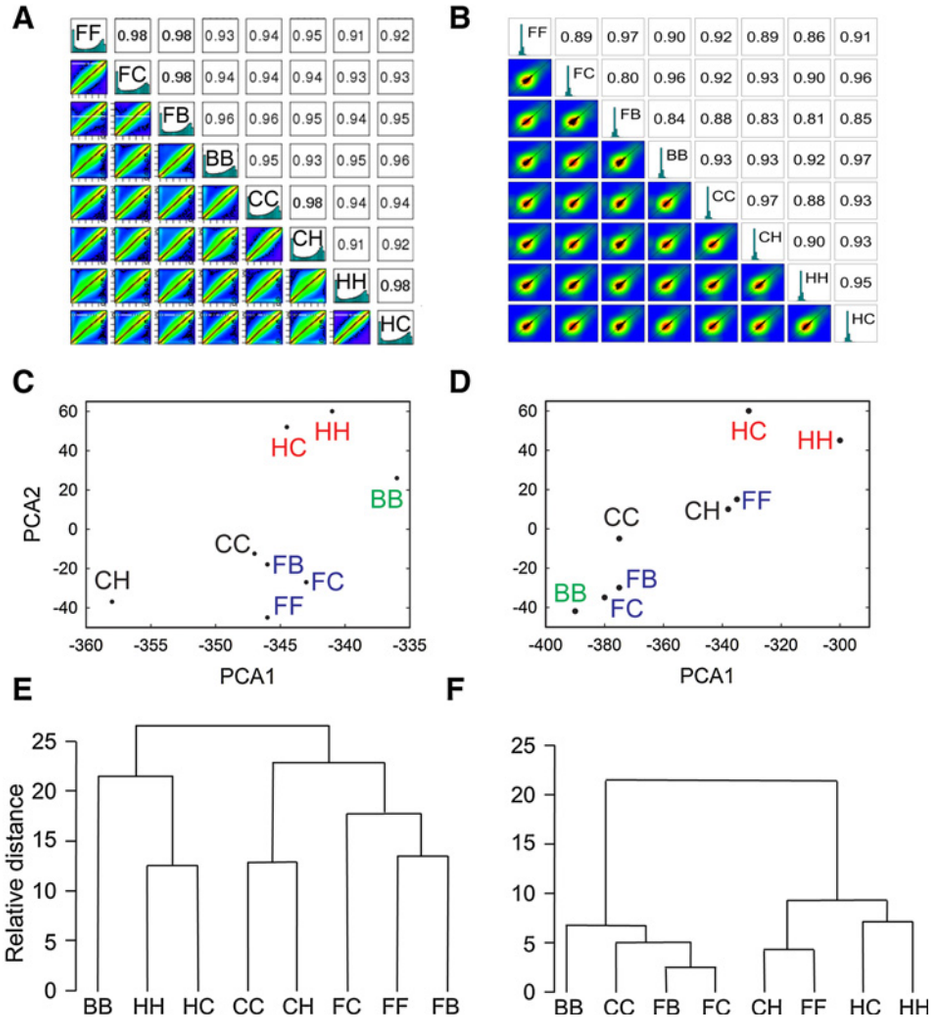

Figure 2.
Methyl-Seq and RNA-Seq comparisons of MNX strains. DNA and RNA samples were collected as described in Fig. 1 from wild-type (FF, BB, CC, HH) and MNX (FB, FC, HC, CH) mice (Mouse strain designations are defined in Table 1). DNA samples were then run on the Agilent SureSelect Mouse Methyl Seq and RNA samples were processed and sequenced using an Illumina Hi-Seq 2500 sequencer. Pearson correlation plots for each of the eight strains (**A** and **B**) show a high level of reproducibility between samples. PCA of wild-type and MNX mouse strains show clustering primarily by nuclear genotype, but MNX strains are distinct for methylation (**C**) and gene expression (**D**). Hierarchical clustering dendrograms also show similar clustering based mostly upon nuclear background for DNA methylation (**E**) and gene expression (**F**).

MNX and wild-type mice differ in gene expression

In tandem, RNA sequencing (RNA-Seq) was performed on total RNA from cerebellum samples from both MNX and wild-type mouse strains using Ilumina HiSeq 2500. Two biological pools were generated from the same samples as used for Methyl-Seq. Quality control metrics were performed and showed good genome-wide coverage and high-quality reads. Similar to between-strain correlations observed with DNA methylation, gene expression measurements were highly correlated between strains and ranged between 0.80 and 0.97 (Fig. 2B). Similarly, sample clustering by nDNA background was observed with respect to the first two principal components (Fig. 2D). Mimicking the PCA results, hierarchical clustering of samples based upon CpG-specific methylation demonstrated a separation of samples according to nuclear background—C57BL/6 (C), C3H/HeN (H), and FVB/N (F) nuclear backgrounds each clustered together (Fig. 2E). Similarly, hierarchical clustering of samples based on gene expression also showed clustering by nuclear background (Fig. 2F), albeit to a lesser degree than was observed for DNA methylation.

Samples with different nuclear backgrounds paired with wild-type mtDNA (from control MNX mice) were compared (e.g., FF vs. CC; FF vs. BB; HH vs. CC). Although the comparisons between wild-type mice were not the focus of our study, they represent the baseline from which to establish the mitochondrial contributions. Comparison of samples with the same mitochondrial background was also done. To directly assess the impact of mtDNA on nuclear DNA methylation and gene expression, the wild-type strains were compared with MNX strains (e.g., FF vs. FC; FF vs. FB; FF vs. FB; CC vs. FC). Three-way comparisons were then performed to identify the unique nuclear genes/CpG loci influenced by the mtDNA. Agilent Sure Select Mouse Methyl-Seq baits were designed to capture 3.7 million CpGs across CpG islands, cancer tissue-specific differentially methylated regions (DMR), Gencode promoters, DMR or regulatory features in CpG islands, shores, and shelves ±4 kb, DNase I hypersensitive sites, Refseq genes and Ensembl regulatory features such as gene bodies (which includes exon 1), CpG islands (CPGI), exons, TSS1500 (1500 base pairs upstream of the transcriptional start site), the 5′-untranslated region (5′-UTR) in exon1, and 3′-untranslated region (3′-UTR). OpenSea refers to anything not falling into the other regulatory categories. Figure 3 visualizes the number and percentage of significantly differentially methylated CpG across each of the considered comparisons by CpG genomic context.

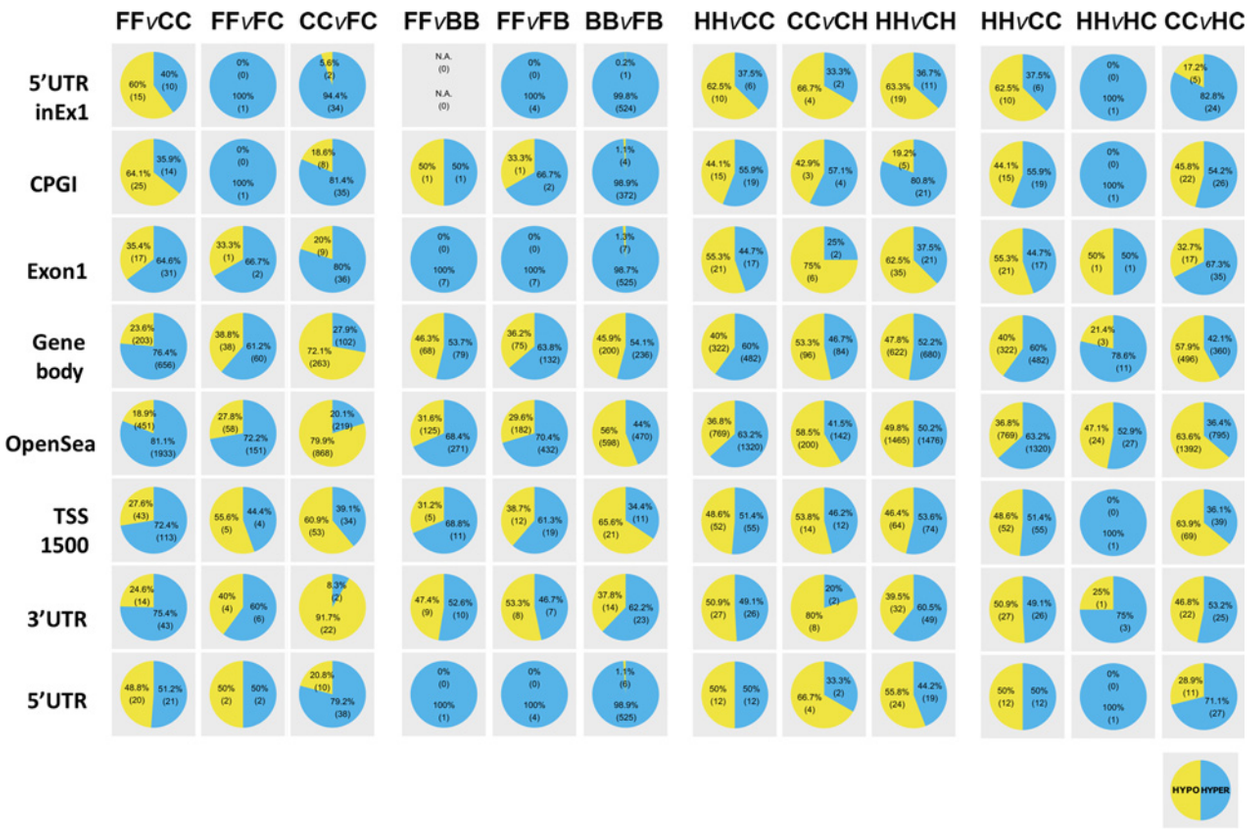

Figure 3.

Changes in DNA methylation in MNX mice by DNA region. DNA collected from brains of wild-type (FF, BB, CC, HH) and MNX (FB, FC, HC, CH) mice (mouse strain designations are defined in Table 1) were analyzed for genome-wide DNA methylation using the SureSelect Methyl-Seq Target Enrichment System. Differential DNA methylation analysis was performed to evaluate 11 comparisons of control and MNX strains. HH v CC is represented twice for visual simplicity with other comparisons. Differentially methylated loci (DML) passing statistical significance (q values < 0.05) and DMV $\geq$ 20 were plotted as pie charts. The values in the pie charts refer to the number (in parentheses) and percentage of differentially hyper- (blue) or hypomethylated (yellow) CpG loci. DML based on genomic context were also summarized in pie charts according to CpG locality in gene body, CpG islands (CPGI), Exon1, TSS 1500, 5′UTR, 3′UTR, 5′UTR (in exon 1), and OpenSea.

While some comparisons showed few or no changes (e.g., 5′-UTR for HH/CC/CH), other comparisons revealed major changes in hypo- or hypermethylation (e.g., CPGI and 3′-UTR for FF/BB/FB). Clear differences in methylation were observed, as expected, between wild-type strains across a broad spectrum of genes, CPGI, and open seas. There were other comparisons, however, which resulted in few differences (e.g., the 5′-UTR between FVB/NJ and BALB/cJ mice). Selected differentially methylated genes from the Meth-Seq were validated by methylation-specific PCR. Genes representing epigenetic regulators (H3f3a, Hdac9, Mbd5, Brd3), metabolism-associated genes (Far1, Atp5f1, Acsf2, Aco1), neuronal function- (Ano2, Myo3a, Ntng1) and metastasis-related genes (Adamts16, Epha6, Serpinb1a) were validated (Supplementary Fig. S1). These data clearly demonstrate that changes in DNA methylation associated with mitochondrial-nuclear pairing are selective rather than genome-wide.

Mitochondria-associated changes in DNA methylation and gene expression are selective

Three-way comparisons of DNA methylation (Fig. 4, blue panels) were also performed to determine the influence of the mitochondrial genome on the nuclear genome. Venn diagrams were generated to represent the intersections between the different comparisons using a q value of $\leq$0.05. Venn diagrams were organized to compare methylation between wild-type strains in the upper circle and nuclear genome driven effects in the bottom right. Values in the nonoverlapping portion of the bottom left circle are the loci specifically influenced by the mitochondrial genome. There were 61 unique hypomethylated loci in the FC, 243 in the FB, 141 in the CH, and 17 in the HC nuclei. There were 113 unique hypermethylated loci in the FC, 492 in FB, 142 in CH, and 27 in the HC nuclei. These large numbers of changes are impressive when considering the relatively small mitochondrial genome compared with the size of the nuclear genome. Note that because any given CpG locus can be annotated to multiple regulatory elements in pie charts there are fewer numbers in the Venn diagrams than are reported in the pie charts (Fig. 3).

Similar three-way comparisons of gene expression are depicted in Fig. 4 (red panels). Again, the bottom left circle shows the number of genes either up- or downregulated that are influenced by the mitochondrial genome. To compare potential expression differences between strains, an arbitrary cutoff of 1.5-fold

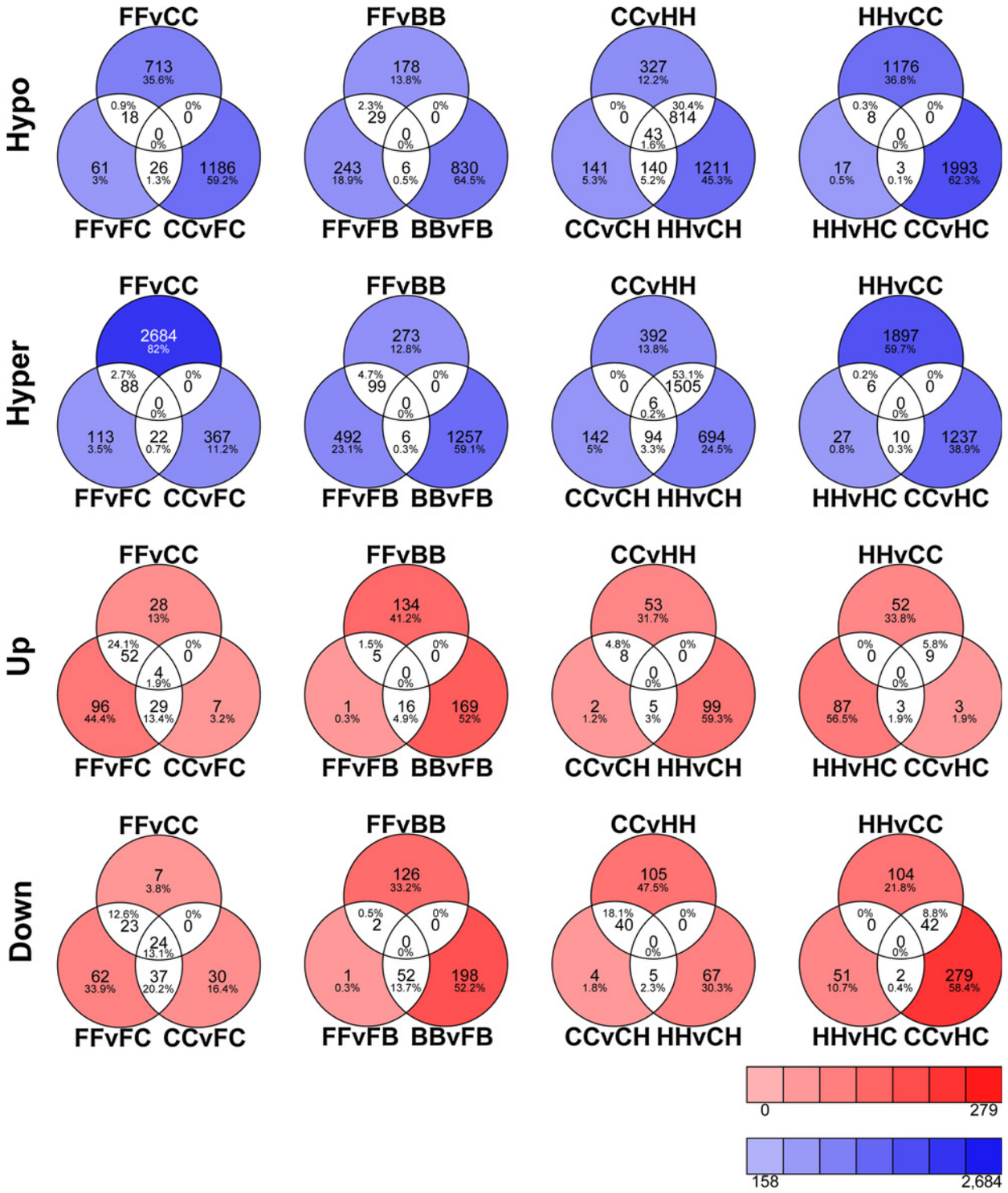

Figure 4.

Selective gene methylation and expression in MNX mice. Differentially methylated and expressed genes in the brains of wild-type (FF, BB, CC, HH) and MNX (FB, FC, HC, CH; mouse strain designations are defined in Table 1) mice were compared and depicted by hypo- or hypermethylation (blue Venn diagrams) and up- or downregulated expression (red Venn diagrams). Three-way comparisons (wild-type for both "parental" strains and the corresponding MNX combination) are shown. The bottom left-hand circle represents the subset of genes differentially methylated or expressed by mtDNA in the MNX mice. Venn diagrams were generated using Venny (http://bioinfogp.cnb.csic.es/tools/venny/index.html).

differential expression was used. There were 96 genes upregulated in FC, 1 upregulated in FB, 2 upregulated in the CH, and 87 upregulated in the HC while there were 62 downregulated in FC, 1 downregulated in FB, 4 downregulated in the CH MNX, and 51 downregulated in the HC. RNA-Seq data are also represented in Volcano plots depicting both upregulated (red panels) and downregulated (green panels) genes (Fig. 5). Two genes "Lars2" and "GU332589" were excluded from the analyses as they exhibited an abnormal behavior (i.e., fold changes in expression were outliers compared with all other genes). As above, selected differentially expressed genes from the RNA-Seq analyses were validated by quantitative PCR using Taqman. Genes representing epigenetic regulators (e.g., Dnmt1, Als2, SatB1, Brd2, Jmjd1c), metabolism-associated genes (e.g., Ogdh, Calb2, Slc8a2, Dgkb, Apod), neuronal function- (e.g., Mpped1, Cpne6, Als2, Nefm, Cdr1) and metastasis-related genes (e.g., Epha4, Fat1, Plk2; Supplementary Fig. S1) were chosen for validation. Ingenuity Pathways Analysis (IPA, http://www.ingenuity.com, Release date: December 2016) revealed 12 different pathways associated with MNX mice. The frequency of identifying a specific pathway from the 11 comparisons performed is shown parenthetically: Huntington's disease (5/11), CREB signaling in neurons (3/11), breast cancer regulation by strathmin (3/11), NFAT in cardiac hypertrophy (3/11), dopamine/DARP32 feedback of cAMP signaling (3/11), glutamate receptor signaling (2/11), protein kinase A (2/11), GPCR signaling (2/11), GABA receptor signaling (2/11), clathrin-mediated endocytosis (2/11), (−) adrenergic signaling (2/11) and synaptic long-term potentiation (2/11). Not unexpectedly, the majority of pathways implicated are involved in neuron function. However, there appears no simplistic explanation for why these pathways are preferentially involved.

Correlation of gene expression to methylation is multifactorial

After observing the changes in gene expression and DNA methylation, we next integrated the findings to determine whether there is a connection between methylation and gene expression. Methylation for the five most differentially expressed genes for which also methylation data were available is shown in Supplementary Fig. S3A–S3K. Expression correlated with DNA methylation in some, but not all, of the genes. Although somewhat unexpected, the lack of direct concordance was not entirely unforeseen. The correlation of gene expression to methylation is multifactorial involving temporal, spatial, and structural regulation. Although it is generally accepted that promoter methylation of CPGI is associated with decreased transcription of downstream genes, DNA methylation in gene bodies has been observed to show the opposite trend and is thought to be a consequence of gene expression rather than a cause (50). Furthermore, studies have shown that degree of gene expression and methylation correlation can be quite modest (50–52). Additionally, coordination with other epigenetic marks (i.e., histone methylation and acetylation status) has not yet been completed and could likely be involved. Nonetheless, the primary conclusion remains true—different mtDNA–nDNA combinations alter nDNA methylation status and correspondingly gene expression. More in-depth integrative analyses are under way with the objective of identifying direct and indirect changes associated with phenotypic differences in the MNX mice.

Many CpG islands transcend many genes and it is noted that certain CpG islands were more commonly affected than others. Our DNA methylation analysis revealed that CPGI 31, 54, 68, 69, 71, 81, 103, 115, 181, and 360 were differentially methylated at a higher frequency than other CPGI loci. The changes, however, were typically associated with crosses with unique nuclear genomes rather than a particular mitochondrial genome strain. Although there are clearly mtDNA-associated changes in CPGI expression patterns, the analysis here was unable to identify discriminating patterns, strongly suggesting strain-specific effects.

Growth, life-span, fecundity, cell-cycle distribution, and basal apoptosis in MNX mice are not different

Among the many genes differentially regulated, some are associated with intermediary metabolism, which is consistent with changes in mitochondria function previously reported in the MNX mice (7, 8). For the most part, MNX strains grew at rates similar to their wild-type counterparts (Fig. 6 shows growth curves for all the MNX strains compared with published growth curve data obtained from Envigo (for the C3H/HeN) or Jackson Laboratories (for the FVB/NJ, C57BL/6J, and BALB/cJ). MNX mice did not exhibit major differences in overall lifespan (Supplementary Fig. S4), litter size or gender ratios (Supplementary Fig. S5) or rates of spontaneous tumor development (data not shown). However, both male and female HC MNX were obese compared with wild-type counterparts, reflecting changes in metabolic protein expression and functionality (Fig. 6A and B), but not cell-cycle distribution (Supplementary Fig. S6) nor apoptotic indices as measured in primary embryo fibroblast cultures (Supplementary Fig. S7).

Discussion

According to current theory, mitochondria were phagocytosed by another single-cell organism. Nuclear and mitochondrial genomes then co-evolved, leading to a symbiotic relationship in eukaryotes. It stands to reason that communication between the two organisms maintains nonpathogenic symbiosis. By altering retrograde signaling that has evolved over several years by introducing a different mitochondrial genome, we show that nuclear-mitochondrial cross-talk is vital. Using the Agilent SureSelect Mouse Methyl Seq protocol, we were able, for the first time, to compare DNA methylation in a genome-wide, unbiased manner in the mouse brain. As our hypothesis predicted, our data demonstrate selective changes in cytosine methylation correlating with mtDNA polymorphisms paired with wild-type nuclei. Importantly, the cells have never been exposed to mutagens as in cybrids nor do they contain residual non-host DNA remaining after backcrossing conplastic strains due to DNA crossover. By extrapolation, interference or manipulation of mitochondrial-nuclear cross-talk would be predicted to contribute to pathologies or, at least, selective alterations in phenotype.

Our findings are consistent with the types of body weight and composition changes recently reported in conplastic C57BL/6-mt(NZB/OlaHsd) mice by Latorre-Pellicer and colleagues (5). They recognized that their data illustrated that interactions between genomes could influence several nonpathologic phenotypes; however, a definitive explanation for such changes was not determined. Our data using the MNX mice confirm and extend their observations by providing a plausible mechanistic explanation. Likewise, data from Bellizzi and colleagues used human cybrids to demonstrate that mtDNA polymorphisms

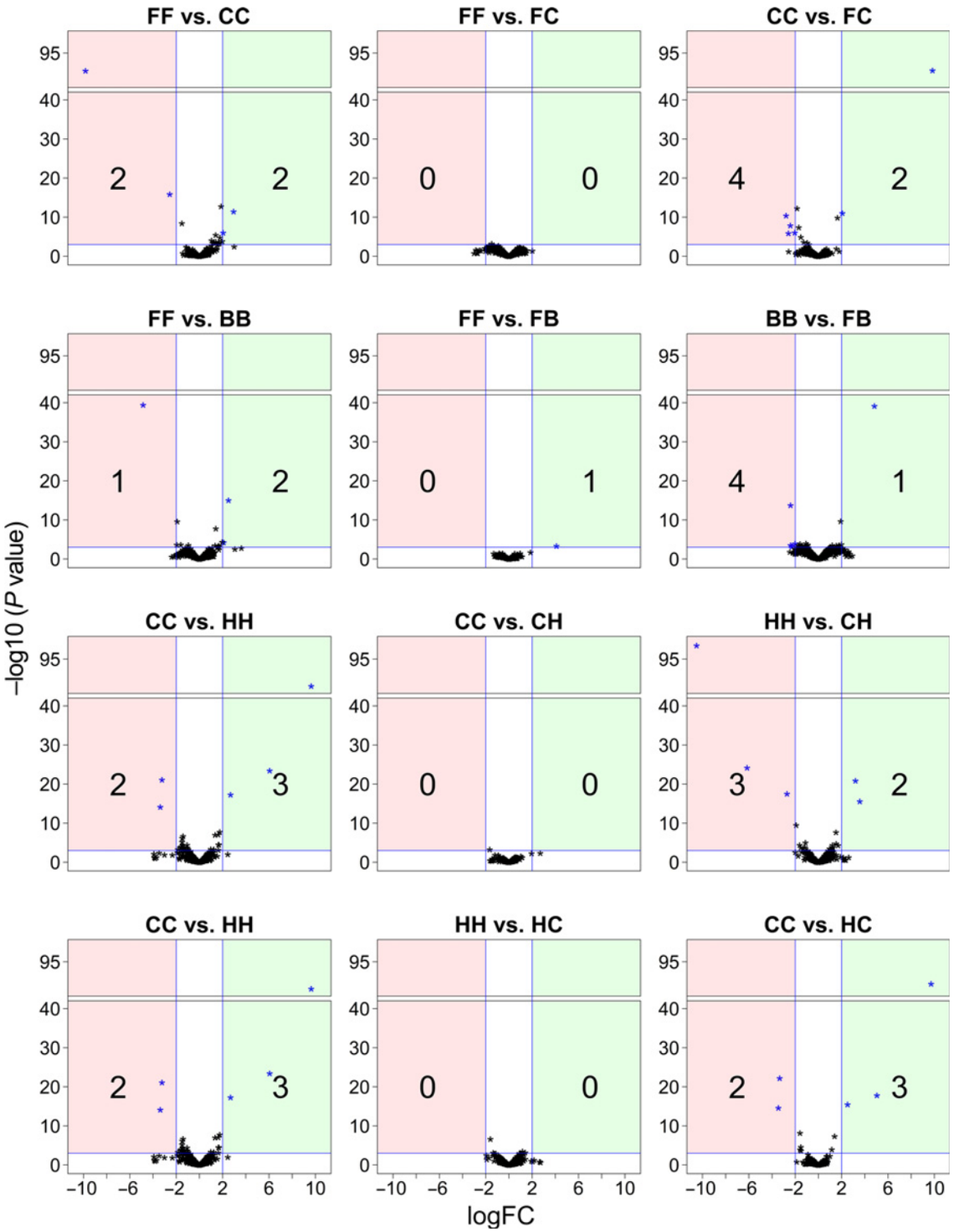

Figure 5.
Differentially expressed genes identified by RNA-Seq in MNX mice. Volcano plots help visualize up- (red) and downregulated (green) gene expression in MNX mice. Specific comparisons are shown for individual genes. The values are the number of genes significantly ($P < 0.05$) differentially regulated. Mouse strain designations are defined in Table 1.

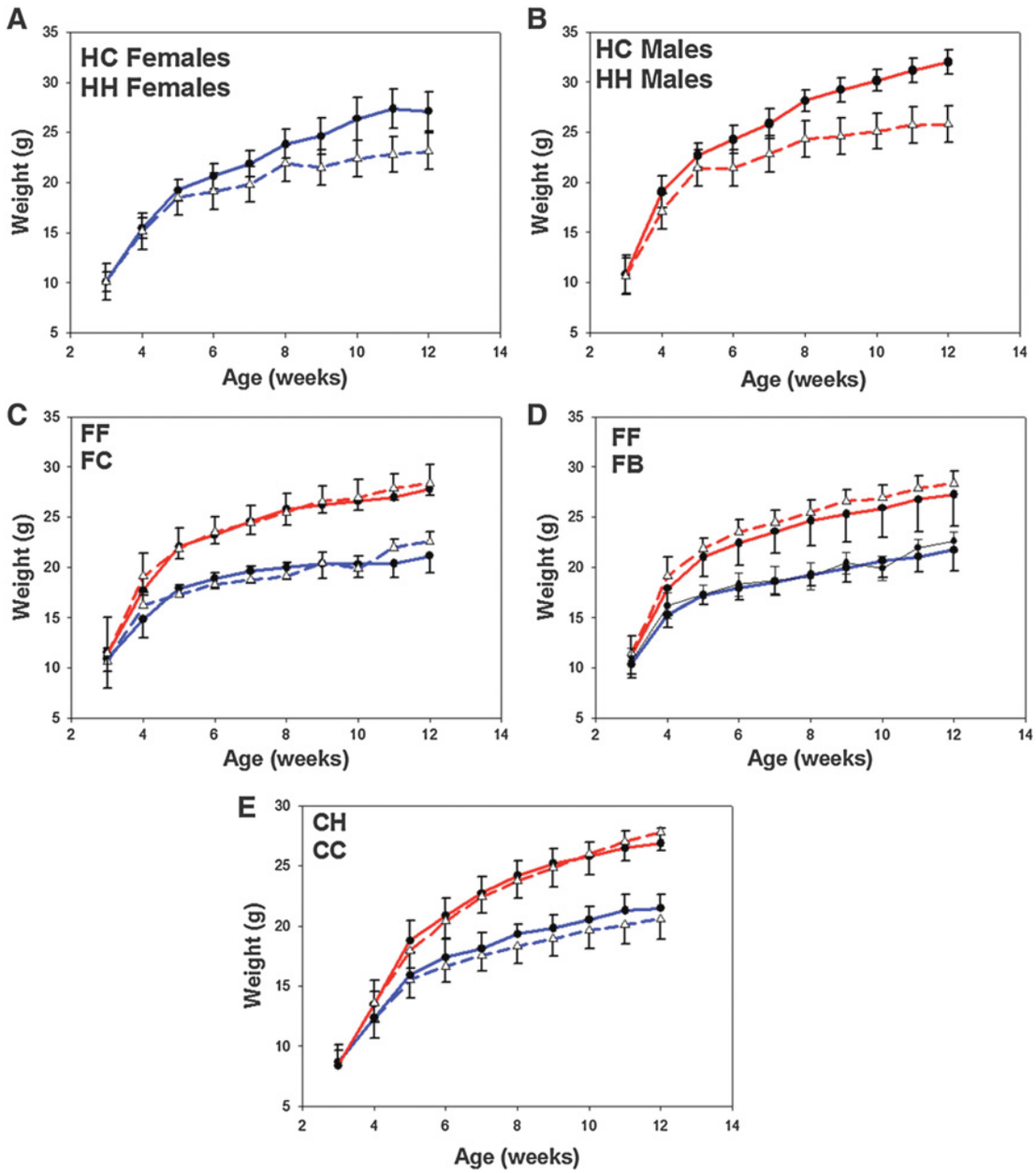

Figure 6.

Mouse growth rates for wild-type and MNX mice. Weighing of male and female mice began after weaning and continued for 9 weeks. Wild-type mouse growth rates were compared with published growth for mice purchased from Envigo (C3H/HeN) or Jackson Labs (C57BL/6J and FVB/NJ). Growth of HC MNX female (**A**) and male (**B**) mice compared with HH wild-type mice. MNX (FC, FB, and CH) mouse growth was compared with wild-type male (red) and female (blue). The solid lines in all panels are MNX mice while the dashed lines are for wild-type. Symbols, mean ± SD (n = 13–30/group). Mouse strain designations are defined in Table 1.

could alter nDNA methylation patterns (53) and the underlying mechanism(s) responsible have not yet been determined.

Subtle changes in metabolism were observed in all MNX strains compared with their wild-type counterparts and may have directly or indirectly led to nDNA methylation changes. For example, by shifting methyl donor pools, DNA methylation status could shift. Although testing this hypothesis is conceptually straightforward, analyses of brain tissue *in situ* is complicated by the need to discriminate which brain regions are being examined. Furthermore, even short-term culturing of cells alters metabolic profiles; so, *in vitro* analyses are of limited value. Experiments to address whether alternative metabolite pools in MNX mice alter nDNA methylation are underway. To date, no consistent metabolite changes have been correlated with changes in the phenotypes

examined. Likewise, Guha and colleagues recently reported that mtDNA copy-number changes were associated with differential histone methylation (54). Although mtDNA copy numbers have fluctuated slightly in the MNX mice over time, there is not a significant change in the MNX mice compared with wild-type (data not shown).

Like humans, mouse phylogenetic trees show divergence into different clades. Inbred mouse strains can be segregated into seven clusters (55). Based upon nuclear and mitochondrial genome sequences, BALB/cJ and C3H/HeN are in the same branch. Similarly, these strains also appear in the same ancestral branch based upon basal methylation and RNA expression patterns. Similarly, C57BL/6J and FVB/NJ cluster in the same branches of the phylogenetic tree for nuclear sequences, expression and methylation. Correspondingly, mtDNA SNPs reflect the different clusters of inbred *M. musculus* strains used for these studies; that is, BALB/cJ and C3H/HeN contain similar SNPs that differ from SNPs found in C57BL/6J and FVB/NJ. Based upon methylation changes and expression profiles, each combination of nDNA and mitochondrial DNA in the MNX mice represents a distinct strain of mouse. Importantly, the strains have remained stable phenotypically for several generations as long as the matrilineal mtDNA is maintained.

Changes in nDNA methylation due to mitochondrial polymorphisms represent one of the many possible epigenetic changes that can occur when nDNA and mtDNA are juxtaposed. That differential methylation occurs throughout the nuclear genome, but is selective, provides an explanation for how mtDNA could alter normal homeostasis as well as susceptibility and/or severity of diseases. Correspondingly, changes in gene expression, as measured by RNA-Seq, revealed a finite list of differentially expressed genes under nonstress conditions.

That mitochondria appear to signal to the nucleus and change epigenetic patterns provides an explanation for how the mitochondrial genome could influence a polygenic phenotype as complex as cancer metastasis (8). It has long been recognized that metastasis requires coordinated expression of dozens of nucleus-encoded genes (56, 57); so, it was implausible that a simple change in mtDNA could alter metastasis directly. Mitochondrion-induced shifts in the nuclear epigenome simply makes sense.

Although our observations and their corresponding conclusions have important biological and disease implications, they also have limitations. First, the studies were performed using only a single tissue type. We chose brain as this tissue is highly metabolic and contains abundant mitochondria. However, metabolic profiles and mitochondrial content vary widely in different tissues, cautioning against extrapolating details from our findings in one tissue to all tissues or cells. Furthermore, different regions of the brain have highly specialized functions that were not assessed here. Second, several reports demonstrate differential tissue methylation in different racial groups (54–56). As the strains of mice mimic racial groups in humans, the findings reported in mice provide a partial, plausible explanation for why the differential methylation exists in tissues from different races. Likewise, the results hint that the MNX mice and the differential methylation may, in part, explain racial disparities in disease susceptibility and progression. Third, microenvironmental factors also change methylation and expression profiles. Although all mice in this study were housed in a controlled environment, microclimates and intrinsic interindividual heterogeneity decrease the signal-to-noise ratio. However, given how reproducible the pools were, we do not think this was a huge factor. The use of pools of mouse brains was intended to mitigate interindividual variability; however, the design could mask relevant changes. Fourth, although DNA methylation is stable and the MNX strains used for the studies reported here utilized mice multiple generations after the foundational MNX mouse (8th filial generation), there can be minor fluctuations between generations depending upon environmental conditions. Thus, the findings here represent only a snapshot in time. Despite these potential limitations, the results reported here are consistent with previous microarray analyses showing that mitochondrial dysfunction in neurons can alter expression of nuclear genes (20). Fifth, despite our best attempts to utilize statistical rigor when analyzing the changes in methylation and expression in the MNX mice compared with their wild-type counterparts, the sample size for the studies presented here is a limiting factor, especially for the integrative analysis of the expression and data sets. Sixth, the identity(ies) of the signal(s) from mitochondria responsible for changes in DNA methylation and gene expression have not yet been determined. In addition to metabolite differences discussed above, ncRNA, tRNA, and tRF, which were once disregarded as useless fragments of RNA, are now increasingly recognized as important (57–59). tRNA represents about 4% to 10% of the total cellular DNA; yet, are the predominate transcripts encoded by mtDNA. It has been shown that tRF can affect gene silencing (57–59).

As a cautionary note, there are diseases known to be driven by mutations in mtDNA, such as Leber's hereditary optic neuropathy and Leigh's syndrome. These mitochondriopathies are caused by mutations in mtDNA-encoded proteins, which, in turn, disrupt numerous metabolic processes and pathways. It is interesting to speculate that disease progression may also be related to mitochondrial regulation of gene methylation and/or expression. Furthermore, recent reports have proposed a strategy using surrogate cytoplasts as carriers for maternal nDNA as a method to prevent such mitochondriopathies (60–62). In essence, these latter approaches are a human therapeutic equivalent of MNX mice. So, although so-called 3-parent babies afford the possibility to resolve an acute disease, there may be unexpected and unwanted consequences as the cross-talk between genomes could lead to changes in gene expression and phenotype. Deeper understanding of the mechanisms by which mitochondria regulate nuclear gene expression will be needed in order to finely tune this treatment strategy. Determining the signal(s) from mitochondria to the nucleus may, thus, provide important clues linking genomic polymorphisms, metabolism, epigenetic regulation, and multiple complex phenotypes.

Disclosure of Potential Conflicts of Interest

No potential conflicts of interest were disclosed.

Authors' Contributions

Conception and design: C.J. Vivian, A.E. Brinker, B. Salhia, D.R. Welch
Development of methodology: G.C. Gooden, B. Salhia, D.R. Welch
Acquisition of data (provided animals, acquired and managed patients, provided facilities, etc.): C.J. Vivian, A.E. Brinker, G.C. Gooden, B. Salhia, D.R. Welch
Analysis and interpretation of data (e.g., statistical analysis, biostatistics, computational analysis): C.J. Vivian, A.E. Brinker, S. Graw, D.C. Koestler, C. Legendre, B. Salhia
Writing, review, and/or revision of the manuscript: C.J. Vivian, A.E. Brinker, D.C. Koestler, C. Legendre, G.C. Gooden, B. Salhia, D.R. Welch

Administrative, technical, or material support (i.e., reporting or organizing data, constructing databases): C.J. Vivian, D.R. Welch
Study supervision: D.R. Welch

Acknowledgments

The authors wish to thank the members of our respective laboratories for insightful comments, critical reading of the manuscript and support as well as Isidore Rigoutsos for constructive conversations. We also acknowledge co-development of the MNX mouse model with Scott Ballinger. The authors also thank the KUMC Genome Sequencing Facility (Clark Bloomer), Transgenic and Gene Targeting Facility (Jay Vivian), Biostatistics Shared Resource and other KU Cancer Center Shared Resources.

Grant Support

This work was generously supported by Susan G. Komen for the Cure (SAC11037 to D.R. Welch) and the National Foundation for Cancer Research (D.R. Welch), with additional support from NIH grants R01-CA134981 (D.R. Welch), P30-CA168524 (D.R. Welch and D.C. Koestler), 1KL2TR000119 (D.C. Koestler), and the Hall Family Professorship in Molecular Medicine (D.R. Welch).

The costs of publication of this article were defrayed in part by the payment of page charges. This article must therefore be hereby marked *advertisement* in accordance with 18 U.S.C. Section 1734 solely to indicate this fact.

Received May 23, 2017; revised June 14, 2017; accepted June 15, 2017; published OnlineFirst June 29, 2017.

References

1. Wallace DC. Mitochondrial DNA variation in human radiation and disease. Cell 2015;163:33–8.
2. Wallace DC, Fan W. Energetics, epigenetics, mitochondrial genetics. Mitochondrion 2010;10:12–31.
3. Wallace DC. A mitochondrial paradigm of metabolic and degenerative diseases, aging, and cancer: a dawn for evolutionary medicine. Ann Rev Genet 2005;39:359–407.
4. Wallace DC. Genetics: mitochondrial DNA in evolution and disease. Nature 2016;535:498–500.
5. Latorre-Pellicer A, Moreno-Loshuertos R, Lechuga-Vieco AV, Sanchez-Cabo F, Torroja C, Acin-Perez R, et al. Mitochondrial and nuclear DNA matching shapes metabolism and healthy ageing. Nature 2016;535:561–5.
6. Richter-Dennerlein R, Oeljeklaus S, Lorenzi I, Ronsor C, Bareth B, Schendzielorz AB, et al. Mitochondrial protein synthesis adapts to influx of nuclear-encoded protein. Cell 2016;167:471–83.
7. Fetterman JL, Zelickson BR, Johnson LW, Moellering DR, Westbrook DG, Pompilius M, et al. Mitochondrial genetic background modulates bioenergetics and susceptibility to acute cardiac volume overload. Biochem J 2013;456:147.
8. Feeley KP, Bray AW, Westbrook DG, Johnson LW, Kesterson RA, Ballinger SW, et al. Mitochondrial genetics regulate breast cancer tumorigenicity and metastatic potential. Cancer Res 2015;75:4429–36.
9. Ballinger SW. Mitochondrial dysfunction in cardiovascular disease. Free Radic Biol Med 2005;38:1278–95.
10. Swerdlow RH. Mitochondria and cell bioenergetics: increasingly recognized components and a possible etiologic cause of Alzheimer's disease. Antioxid Redox Signal 2012;16:1434–55.
11. Wilkins HM, Carl SM, Swerdlow RH. Cytoplasmic hybrid (cybrid) cell lines as a practical model for mitochondriopathies. Redox Biol 2014;2C:619–31.
12. Patananan AN, Wu TH, Chiou PY, Teitell MA. Modifying the mitochondrial genome. Cell Metab 2016;23:785–96.
13. Arruda AP, Pers BM, Parlakgul G, Guney E, Inouye K, Hotamisligil GS. Chronic enrichment of hepatic endoplasmic reticulum-mitochondria contact leads to mitochondrial dysfunction in obesity. Nat Med 2014;20:1427–35.
14. Berridge MV, Dong L, Neuzil J. Mitochondrial DNA in tumor initiation, progression, and metastasis: role of horizontal mtDNA transfer. Cancer Res 2015;75:3203–8.
15. Dang CV. Links between metabolism and cancer. Genes Dev 2012;26:877–90.
16. Kesterson RA, Johnson LW, Lambert LJ, Vivian JL, Welch DR, Ballinger SW. Generation of mitochondrial-nuclear eXchange mice via pronuclear transfer. Bio Protoc 2016;6:piii:e1976.
17. Horan MP, Cooper DN. The emergence of the mitochondrial genome as a partial regulator of nuclear function is providing new insights into the genetic mechanisms underlying age-related complex disease. Hum Genet 2014;133:435–58.
18. Castegna A, Iacobazzi V, Infantino V. The mitochondrial side of epigenetics. Physiol Genomics 2015;47:299–307.
19. Poyton RO, McEwen JE. Crosstalk between nuclear and mitochondrial genomes. Annu Rev Biochem 1996;65:563–607.
20. Cagin U, Enriquez JA. The complex crosstalk between mitochondria and the nucleus: what goes in between? Int J Biochem Cell Biol 2015;63:10–5.
21. Butow RA, Avadhani NG. Mitochondrial signaling: the retrograde response. Mol Cell 2004;14:1–15.
22. Jazwinski SM. The retrograde response: a conserved compensatory reaction to damage from within and from without. Prog Mol Biol Transl Sci 2014;127:133–54.
23. Suzuki MM, Bird A. DNA methylation landscapes: provocative insights from epigenomics. Nat Rev Genet 2008;9:465–76.
24. Kinnaird A, Zhao S, Wellen KE, Michelakis ED. Metabolic control of epigenetics in cancer. Nat Rev Cancer 2016;16:694–707.
25. Liu F, Wang L, Perna F, Nimer SD. Beyond transcription factors: how oncogenic signalling reshapes the epigenetic landscape. Nat Rev Cancer 2016;16:359–72.
26. Portela A, Esteller M. Epigenetic modifications and human disease. Nat Biotechnol 2010;28:1057–68.
27. Iacobazzi V, Castegna A, Infantino V, Andria G. Mitochondrial DNA methylation as a next-generation biomarker and diagnostic tool. Mol Genet Metab 2013;110:25–34.
28. Tognini P, Napoli D, Tola J, Silingardi D, Della RF, D'Esposito M, et al. Experience-dependent DNA methylation regulates plasticity in the developing visual cortex. Nat Neurosci 2015;18:956–8.
29. Geybels MS, Alumkal JJ, Luedeke M, Rinckleb A, Zhao S, Shui IM, et al. Epigenomic profiling of prostate cancer identifies differentially methylated genes in TMPRSS2:ERG fusion-positive versus fusion-negative tumors. Clin Epigenetics 2015;7:128.
30. Geybels MS, Zhao S, Wong CJ, Bibikova M, Klotzle B, Wu M, et al. Epigenomic profiling of DNA methylation in paired prostate cancer versus adjacent benign tissue. Prostate 2015;75:1941–50.
31. Li E, Beard C, Jaenisch R. Role for DNA methylation in genomic imprinting. Nature 1993;366:362–5.
32. Reik W. Stability and flexibility of epigenetic gene regulation in mammalian development. Nature 2007;447:425–32.
33. Zemach A, McDaniel IE, Silva P, Zilberman D. Genome-wide evolutionary analysis of eukaryotic DNA methylation. Science 2010;328:916–9.
34. Li M, Hong G, Cheng J, Li J, Cai H, Li X, et al. Identifying reproducible molecular biomarkers for gastric cancer metastasis with the aid of recurrence information. Sci Rep 2016;6:24869.
35. Li S, Mason CE, Melnick A. Genetic and epigenetic heterogeneity in acute myeloid leukemia. Curr Opin Genet Dev 2016;36:100–6.
36. Ghosh S, Sengupta S, Scaria V. Comparative analysis of human mitochondrial methylomes shows distinct patterns of epigenetic regulation in mitochondria. Mitochondrion 2014;18:58–62.
37. van der Wijst MG, Rots MG. Mitochondrial epigenetics: an overlooked layer of regulation? Trends Genet 2015;31:353–6.
38. Bunkar N, Bhargava A, Khare NK, Mishra PK. Mitochondrial anomalies: driver to age associated degenerative human ailments. Front Biosci (Landmark Ed) 2016;21:769–93.
39. Chinnery PF, Elliott HR, Hudson G, Samuels DC, Relton CL. Epigenetics, epidemiology and mitochondrial DNA diseases. Int J Epidemiol 2012;41:177–87.

40. Strakova A, Ni LM, Wang GD, Yin TT, Airikkala-Otter I, Allen JL, et al. Mitochondrial genetic diversity, selection and recombination in a canine transmissible cancer. eLIFE 2016;5:piii:e14552.
41. Elmer GI, Pieper JO, Hamilton LR, Wise RA. Qualitative differences between C57BL/6J and DBA/2J mice in morphine potentiation of brain stimulation reward and intravenous self-administration. Psychopharmacology (Berl) 2010;208:309–21.
42. Bai RK, Leal SM, Covarrubias D, Liu A, Wong LJC. Mitochondrial genetic background modifies breast cancer risk. Cancer Res 2007;67:4687–94.
43. Minocherhomji S, Tollefsbol TO, Singh KK. Mitochondrial regulation of epigenetics and its role in human diseases. Epigenetics 2012;7:326–34.
44. Antequera F, Bird A. Number of CpG islands and genes in human and mouse. Proc Natl Acad Sci 1993;90:11995–9.
45. Krueger F, Andrews SR. Bismark: a flexible aligner and methylation caller for Bisulfite-Seq applications. Bioinformatics 2011;27:1571–2.
46. Li LC, Dahiya R. MethPrimer: designing primers for methylation PCRs. Bioinformatics 2002;18:1427–31.
47. Tognini P, Napoli D, Pizzorusso T. Dynamic DNA methylation in the brain: a new epigenetic mark for experience-dependent plasticity. Front Cell Neurosci 2015;9:331.
48. Sanchez-Mut JV, Aso E, Panayotis N, Lott I, Dierssen M, Rabano A, et al. DNA methylation map of mouse and human brain identifies target genes in Alzheimer's disease. Brain 2013;136:3018–27.
49. Katz TA, Liao SG, Palmieri VJ, Dearth RK, Pathiraja TN, Huo Z, et al. Targeted DNA Methylation Screen in the Mouse Mammary Genome Reveals a Parity-Induced Hypermethylation of Igf1r That Persists Long after Parturition. Cancer Prev Res (Phila) 2015;8:1000–9.
50. Gutierrez-Arcelus M, Lappalainen T, Montgomery SB, Buil A, Ongen H, Yurovsky A, et al. Passive and active DNA methylation and the interplay with genetic variation in gene regulation. eLIFE 2013;2:e00523.
51. Jung S, Kim S, Gale M, Cherni I, Fonseca R, Carpten J, et al. DNA methylation in multiple myeloma is weakly associated with gene transcription. PLoS One 2012;7:e52626.
52. Legendre CR, Demeure MJ, Whitsett TG, Gooden GC, Bussey KJ, Jung S, et al. Pathway Implications of Aberrant Global Methylation in Adrenocortical Cancer. PLoS One 2016;11:e0150629.
53. Bellizzi D, D'Aquila P, Giordano M, Montesanto A, Passarino G. Global DNA methylation levels are modulated by mitochondrial DNA variants. Epigenomics 2012;4:17–27.
54. Guha M, Srinivasan S, Ruthel G, Kashina AK, Carstens RP, Mendoza A, et al. Mitochondrial retrograde signaling induces epithelial-mesenchymal transition and generates breast cancer stem cells. Oncogene 2014;33:5238–50.
55. Petkov PM, Ding Y, Cassell MA, Zhang W, Wagner G, Sargent EE, et al. An efficient SNP system for mouse genome scanning and elucidating strain relationships. Genome Res 2004;14:1806–11.
56. Kang YB, Siegel PM, Shu WP, Drobnjak M, Kakonen SM, Cordón-Cardo C, et al. A multigenic program mediating breast cancer metastasis to bone. Cancer Cell 2003;3:537–49.
57. Eccles SA, Welch DR. Metastasis: recent discoveries and novel treatment strategies. Lancet 2007;369:1742–57.
58. Telonis AG, Kirino Y, Rigoutsos I. Mitochondrial tRNA-lookalikes in nuclear chromosomes: could they be functional? RNA Biol 2015;12:375–80.
59. Telonis AG, Loher P, Honda S, Jing Y, Palazzo J, Kirino Y, et al. Dissecting tRNA-derived fragment complexities using personalized transcriptomes reveals novel fragment classes and unexpected dependencies. Oncotarget 2015;6:24797–822.
60. Craven L, Tuppen HA, Greggains GD, Harbottle SJ, Murphy JL, Cree LM, et al. Pronuclear transfer in human embryos to prevent transmission of mitochondrial DNA disease. Nature 2010;465:82–5.
61. Chinnery PF, Craven L, Mitalipov S, Stewart JB, Herbert M, Turnbull DM. The challenges of mitochondrial replacement. PLoS Genet 2014;10:e1004315.
62. Ma H, Folmes CD, Wu J, Morey R, Mora-Castilla S, Ocampo A, et al. Metabolic rescue in pluripotent cells from patients with mtDNA disease. Nature 2015;524:234–8.